IN-CREVICE CHEMISTRY MODEL DEVELOPMENT FOR NICKEL-BASED ALLOYS AND ANALYSIS OF MODEL RESULTS IN VIEW OF LITERATURE INFORMATION

Prepared for

U.S. Nuclear Regulatory Commission
Contract NRC–02–07–006

Prepared by

P. Shukla
R. Pabalan
X. He

Center for Nuclear Waste Regulatory Analyses
San Antonio, Texas

September 2011

ABSTRACT

This report documents previously unpublished information on the topic of model development for understanding in-crevice chemistry and analysis of model results.

In the Yucca Mountain Safety Analysis Report, the U.S. Department of Energy assumed that, once initiated, the localized corrosion in form of crevice corrosion of Alloy 22 will keep on propagating as long as corrosion potential is higher than the crevice corrosion for repassivation potential. In order to better understand the propagation behavior of crevice corrosion in Alloy 22, the Center for Nuclear Waste Regulatory Analyses staff developed a physico-chemical model to determine the chemical environment that could develop inside a crevice. The model results indicated that both cations' and anions' concentrations are likely to be higher than the ions' concentration in the bulk solution residing outside the crevice. Furthermore, the in-crevice solution is expected to be more acidic than the bulk solution.

Literature information was compiled to understand implications of the model results. Specifically, the model results were analyzed in view of the literature information that provided corrosion rate of Alloy 22 in different acidic chemical environments. The literature information indicated that accelerated corrosion of the alloy will take place in a solution as long as the solution pH is below a threshold value, which is predominantly a function of chloride and nitrate concentrations, and temperature. The combined analysis of literature information and model results indicate that crevice corrosion process is unlikely to stifle due to evolution of in-crevice chemical environment.

CONTENTS

Section Page

FIGURES

Figure Page

TABLES

Table Page

ACKNOWLEDGMENTS

This report describes work performed by the Center for Nuclear Waste Regulatory Analyses (CNWRA®) for the U.S. Nuclear Regulatory Commission (USNRC) under Contract No. NRC–02–07–006. The activities reported here were performed on behalf of the USNRC Office of Nuclear Material Safety and Safeguards, Division of High-Level Waste Repository Safety. This report is an independent product of CNWRA and does not necessarily reflect the view or regulatory position of USNRC.

The authors gratefully acknowledge H. Jung for his technical review, T. Mintz for his programmatic and editorial reviews, and A. Ramos for his administrative support.

QUALITY OF DATA, ANALYSES, AND CODE DEVELOPMENT

DATA: All CNWRA-generated original data contained in this report meet the quality assurance requirements described in the Geosciences and Engineering Division Quality Assurance Manual. Sources for other data should be consulted for determining the level of quality for those data. Computational calculations have been recorded in CNWRA Scientific Notebook 1003E (Shukla, 2009).

ANALYSES AND CODES: This report includes results of calculations performed using OLI Analyzer Studio (OLI Systems, Inc., 2010)—commercially available software maintained in accordance with CNWRA Technical Operating Procedure (TOP)–018, Development and Control of Scientific and Engineering Software. Other computations and plotting were accomplished using Matlab® (The MathWorks, Inc., 2008).

References

OLI Systems, Inc. "A Guide to Using OLI Analyzer Studio Version 3.1." Morris Plains, New Jersey: OLI Systems, Inc. 2010.

The MathWorks, Inc. "MATLAB Version 7.7.0.471 (R20008b)." Natick, Massachusetts: The MathWorks, Inc. 2008.

Shukla, P. Scientific Notebook No. 1003E. San Antonio, Texas: CNWRA. 2009.

1 INTRODUCTION

This report is part of the knowledge management activities for the U.S. Nuclear Regulatory Commission high-level waste repository safety program. The two main purposes of this report are (i) to document a previously unpublished description of a physico-chemical process model developed to estimate the concentration of chemical species inside a crevice and (ii) to complete the evaluation of a set of model results for in-crevice chemistry of Alloy 22 by comparing the results with information obtained from the open literature.

The long lifetime of Alloy 22 (Ni–22Cr–13Mo–4Fe–3W) waste packages is an important attribute of the proposed high-level waste repository at Yucca Mountain, Nevada (DOE, 2002) to isolate nuclear waste from the geosphere. The chemical degradation (i.e., corrosion) of the waste package material is considered to be an important process that could limit the life of waste package materials. More specifically, the localized corrosion in form of crevice corrosion is one of the degradation processes that could limit the life of the waste package. In the Yucca Mountain Safety Analysis Report (DOE, 2008), the U.S. Department of Energy (DOE) assumed that, once initiated, the crevice corrosion of Alloy 22 will keep on propagating as long as corrosion potential is higher than the crevice corrosion for repassivation potential. To evaluate whether crevice corrosion would continue to propagate or stifle, the Center for Nuclear Waste Regulatory Analyses (CNWRA) staff developed a physico-chemical model to determine a range of chemical environments that could develop inside a crevice.

Nickel-based alloys, such as Alloy 600 and C–276, exhibit superior localized corrosion (Kirk and Othmer, 1997) resistance compared to iron-based alloys, such as stainless steel. Nickel-based alloys can be susceptible to localized corrosion in the form of crevice corrosion when the corrosion potential is greater than the repassivation potential in a given environment (Gordon, 2002). The severity of localized-corrosion-induced damage on the metal surface is dependent on the evolution of the crevice region chemical environment. Several experimental studies have been conducted to determine the metal dissolution rate in the crevice region (Dunn et. al., 2005; He and Dunn, 2007; He, et al., 2007; Hua and Gordon, 2004; Priyantha et al, 2005). However, the experimental studies do not provide a description of the chemical environment that would develop inside a crevice because of the restricted geometry of the crevices. Furthermore, the experimental studies provide only limited term propagation rate data of the localized corrosion front.

Few studies have been conducted to determine the evolution of the chemical environment inside a crevice of nickel and nickel-based alloys. Harb and Alkire, (1991) developed a process model to simulate the dissolution of a hemispherical corrosion pit on nickel in 0.5 M NaCl. The model accounted for multiple species in solution, reaction equilibria, migration, and surface kinetics. In particular, the Harb and Alkire model accounted for complexation of nickel with chloride. The model results indicated the buildup of nickel and chloride ions inside the pit. Hoffmeister (2004) determined the distribution of dissolved oxygen concentration, chloride concentration, and pH of the in-crevice solution. However, Hoffmeister's work was based upon empirical correlations developed from experimental studies. Watson and Postlethwaite, (1990) developed a physico-chemical process model to determine the chemical environment inside a crevice for Inconel 625 in chloride-containing solutions. Evitts, et al. (1993) simulated the Watson and Postlethwaite model for Inconel 625 at high temperatures to determine the effect of corrosion on the initiation of crevice corrosion. To the authors' best knowledge, no study has been reported that illustrates the range of chemical solutions that could develop inside a crevice on Alloy 22 in the proposed repository environments.

The following approach is adopted to evaluate whether localized corrosion would continue to propagate or stifle. The physico-chemical model to determine the chemical environment range in a crevice is developed by imposing the mass balance for reacting and nonreacting chemical species, and by imposing charge conservation. More specifically, the model considers the transport of two nonreacting anionic species into a crevice and accounts for a metal dissolution, water dissociation, and a metal hydroxide formation reactions inside the crevice. The model equations are solved using an iterative method in which the governing equations for potential and chemical species' distributions are solved independently. The model is implemented for Alloy 22 in the proposed repository environment. Model results are presented for different parameters' values related to the metal dissolution and metal hydroxide reactions. Following the modeling work, literature information is compiled on Alloy 22 corrosion in chemical solutions suggested by the model results. The model results and literature information on Alloy 22 corrosion are analyzed to assess the stifling of the localized corrosion process. To the authors' best knowledge, this approach for evaluating crevice corrosion stifling has not been presented elsewhere.

The report is organized into four chapters. Chapter 1 introduces the technical background and motivation for this topic. Chapter 2 provides a detailed description of the physico-chemical process model. Chapter 3 summarizes the information compiled from the open literature that was used to understand the corrosion rate of Alloy 22 in the chemical solutions that were representative of the in-crevice chemistry indicated by model results. Chapter 4 develops a combined analysis of model results and literature information and presents the conclusions.

2 MODEL DEVELOPMENT

2.1 Description of the Model

The physico-chemical model is developed for a rectangular crevice of length *L,* width *a,* and unit depth. A schematic diagram representing the crevice region and outside the crevice region is presented in Figure 2-1.

A nickel-based alloy is assumed to be immersed in a solution containing chloride, nitrate, and sodium ions. It is assumed the primary metal dissolution reaction in the crevice is the dissolution of nickel, represented by the following chemical equation

$$Ni \rightarrow Ni^{2+} + 2e^{-} \tag{2-1}$$

Chemical composition of a typical mill-annealed Alloy 22 is provided in Table 2-1 (Chiang, et al., 2007). Most nickel-based alloys, such as Alloy 22, also contain chromium and iron in substantial amounts, and dissolution of chromium and iron are also likely in the crevice environment according to the following chemical equations

$$Cr \rightarrow Cr^{3+} + 3e^{-} \tag{2-2}$$

$$Fe \rightarrow Fe^{2+} + 2e^{-} \tag{2-3}$$

However, insight gained regarding the in-crevice chemistry by just considering dissolution of the nickel is expected to be the same as one obtained by considering dissolution of nickel, chromium, and iron. This point is further explained in this section.

The corrosion current density associated with the dissolution of nickel is given by the following equation

$$i_{Ni^{2+}} = \bar{i} \exp\left[\beta\left(V - \Phi\right)\right] \tag{2-4}$$

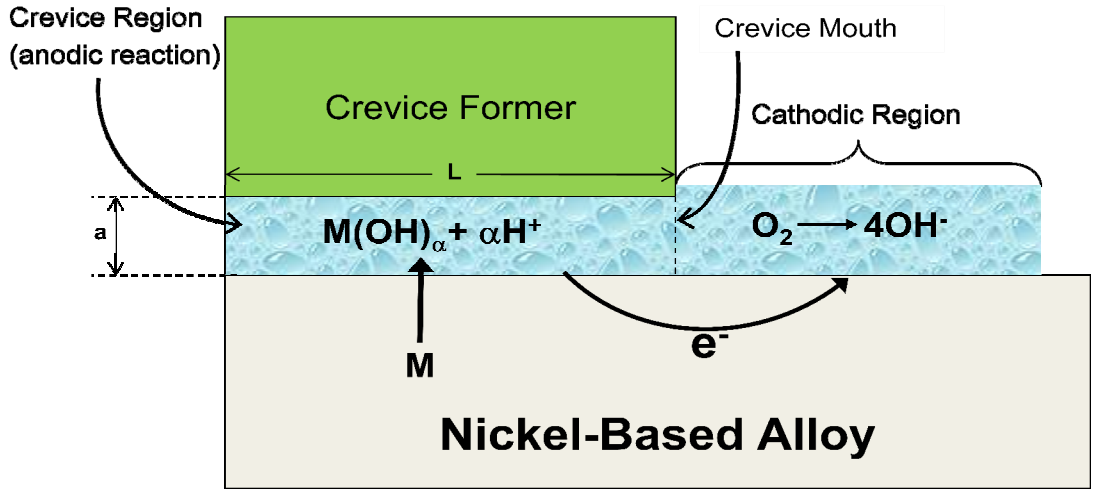

Figure 2-1. Schematic Diagram of the Crevice Corrosion Process for a Nickel-Based Alloy. The Anodic Reaction in the Crevice Region, Which Is Directly Under the Crevice Former, Is the Nickel Dissolution, Whereas Cathodic Reaction in the Cathodic Region Is the Oxygen Reduction.

Table 2-1. Chemical Composition of Mill-Annealed Alloy 22 (in Weight Percent)											
Ni*	**Cr***	**Mo***	**W***	**Fe***	**Co***	**Si***	**Mn***	**V***	**P***	**S***	**C***
56.472	22.15	12.90	2.81	3.82	1.37	0.01	0.30	0.15	0.012	0.002	0.004
*Ni—nitrogen; Cr—chromium; Mo—molybdenum; W—tungsten; Fe—iron; Co—cobalt; Si—silicon; Mn—manganese; V—vanadium; P—phosphorous; S—sulfur; C—carbon											

where

$i_{Ni^{2+}}$ — corrosion current density associated with the dissolution of nickel (A/cm^2)
$\bar{i}$ — equilibrium current density (A/cm^2)
β — inverse of Tafel slope (V^{-1})
V — metal potential (V)
Φ — solution potential (V)

The dissolved nickel ion hydrolyzes to form nickel hydroxide and hydrogen ions according to the following reversible chemical reaction

$$Ni^{2+} + H_2O \Leftrightarrow NiOH^+ + H^+ \tag{2-5}$$

The equilibrium constant for Eq. (2-5) is represented by the following equation

$$K_{eq,N_i} = \frac{C_{NiOH^+} C_{H^+}}{C_{Ni^{2+}}} \tag{2-6}$$

where

K_{eq,N_i} — equilibrium constant of the hydrolysis of the nickel ions (mol/cm^3)
C_{NiOH^+} — concentration of $NiOH^+$ ions (mol/cm^3)
C_{H^+} — concentration of H^+ ions (mol/cm^3)
$C_{Ni^{2+}}$ — concentration of Ni^{2+} ions (mol/cm^3)

Similar to hydrolysis of nickel ions, the hydrolysis of chromium and iron ions would also result in formation of hydrogen ions according to the following chemical reactions

$$Cr^{3+} + H_2O \Leftrightarrow CrOH^{2+} + H^+ \tag{2-7}$$

$$Fe^{2+} + H_2O \Leftrightarrow FeOH^+ + H^+ \tag{2-8}$$

The resulting effect of the above two chemical reactions is additional formation of hydrogen ions, which is already included in the model by considering hydrolyses of nickel ions. Thus, exclusion of chromium and iron dissolution reactions [Eqs. (2-2) and 2-3)], and corresponding metal ions' hydrolyses reactions [Eqs. (2-7) and 2-8)] in the model is not expected to limit the model's ability in providing insight regarding the in-crevice chemistry.
There is scarcity of data in literature on rate constant of metal ion hydrolysis reactions, however, available data on metal ion hydrolysis suggests that the metal ion hydrolysis reactions are rapid compared to metal dissolution reactions, therefore, the nickel ion hydrolysis reaction is judged to be rapid compared to the nickel dissolution and transport of nickel ions via diffusion and migration (Baes and Mesmer, 1979) in the crevice region.

The hydrogen ions, produced ion by Eq. (2-5), equilibrate with the hydroxyl ions according to the following water dissociation reaction

$$H_2O \Leftrightarrow H^+ + OH^- \tag{2-9}$$

The equilibrium constant for the water dissociation reaction is presented by the following equation

$$K_{H_2O} = C_{H^+} C_{OH^-} \tag{2-10}$$

where

K_{H_2O} — equilibrium constant for the water dissociation reaction (mol^2/cm^6)
C_{OH^-} — hydroxyl ion concentration (mol/cm^3)

The ionic species present in the crevice region are sodium, chloride, nitrate, nickel, nickel hydroxide, hydrogen, and hydroxyl ions. The steady-state concentration distribution of these ionic species in the crevice is represented by the following equation

$$-\nabla \cdot N_k + R_k = 0 \tag{2-11}$$

where

R_k — rate of generation of ionic species k ($mol/sec\text{-}cm^3$)
N_k — flux of ionic species k ($mol/sec\text{-}cm^2$)

The flux of an ionic species, N_k, in the solution is represented by the following Nernst-Plank equation

$$N_k = -z_k u_k F C_k \nabla \Phi - D_k \nabla C_k \tag{2-12}$$

where

z_k — charge number of species k
u_k — mobility of species k ($cm^2/sec\text{-}volt$)
F — Faraday constant = 96,486 C/mol
C_k — Concentration of species k (mol/cm^3)
Φ — electrolyte potential (volts)
D_k — diffusion coefficient of species k (cm^2/sec)

It is assumed that the concentrations of various species inside the crevice are low enough to invoke the dilute solution approximation. As a result of the dilute solution approximation, the diffusion coefficient and mobility of a chemical species k are related according to the following equation

$$D_k = u_k RT \tag{2-13}$$

where

R — universal gas constant = 8.3145 J/K/mol
T — temperature of the system (K)

It is further assumed that the crevice solution is electrically neutral. This ensures that no charge separation occurs due to the solution potential gradients in the crevice region

$$\sum_k z_k C_k = 0 \tag{2-14}$$

The model is developed for bulk solution containing sodium, chloride, and nitrate ions. The nickel and nickel hydroxide ions will diffuse in the bulk solution from the crevice region where they are generated. It is assumed that the concentrations of sodium, chloride, nitrate, nickel, nickel hydroxide, hydrogen, and hydroxyl ions at the mouth of the crevice are assumed to be equal to the bulk solution concentration:

$$C_k = C_{k,bulk} \tag{2-15}$$

At the end of the crevice, the flux of the nickel ion concentration is given by the following equation:

$$N_{Ni^{2+}} \cdot \vec{n} = \frac{i_{Ni^{2+}}}{2F} \tag{2-16}$$

where $\vec{n}$ is the outward normal vector. The flux of all other species at the end of the crevice is zero. In this model, it is assumed that no cathodic reaction occurs inside the crevice and the oxygen reduction reaction is the cathodic reaction that occurs outside the crevice, as depicted in Figure 2-1.

2.2 Model Solution Method

Because the width of a crevice is negligible compared to the length of a crevice, it is assumed that concentration gradients across the width of the crevice are also negligible compared to those along the length of the crevice. This assumption is consistent with the approach Alkire and Siittari (1979) adapted to model potential and concentration distributions inside a pit where pit radius was one third of the pit's depth. Under this assumption, the governing equation for concentration distribution labeled Eq. (2-12), can be rewritten as

$$\nabla \cdot N_k = R_k + \frac{N_{sk}}{a} \tag{2-17}$$

where

a — width of the crevice (cm)
N_{sk} — flux of the species k at the metal-solution interface (mol/sec-cm^2)

Note that the operator ∇ is equal to $\frac{d}{dx}$ where x denotes the distance down the crevice from the crevice mouth. The flux of the nickel ions at the metal-solution interface in the crevice region is given by the following equation

$$N_{sNi^{2+}} \cdot \vec{n} = \frac{i_{Ni^{2+}}}{2F} \tag{2-18}$$

where $\vec{n}$ is the outward normal vector. The flux of all other species at the metal-solution interface is zero.

The diffusion and migration of the ionic species in the crevice region generates current. The total current density is defined by

$$i = F\sum_{k=1}^{N} z_k N_k \tag{2-19}$$

and the divergence of the current is given by

$$\nabla \cdot i = \frac{i_{Ni^{2+}}}{2Fa} \tag{2-20}$$

Insertion of Eqs. (2-12) and (2-17) in Eq. (2-18) yields

$$\nabla \cdot \left(\kappa \nabla \Phi\right) + F\sum_{k=1}^{N} z_i \nabla \cdot \left(D_i \nabla C_i\right) = -\frac{i_{Ni^{2+}}}{2Fa} \tag{2-21}$$

where

$$\kappa = F^2 \sum_{k=1}^{N} \frac{z_k^2 D_k C_k}{RT} \tag{2-22}$$

Rearrangement of Eq. (2-21) yields

$$\kappa \nabla^2 \Phi + \nabla \Phi \cdot \nabla \kappa = -\frac{i_{Ni^{2+}}}{2Fa} - F\sum_{k=1}^{N} z_k \nabla \cdot \left(D_k \nabla C_k\right) \tag{2-23}$$

Based upon the stoichiometry of homogeneous chemical reactions given by Eqs. (2-5) and (2-9), it is recognized that

$$R_{Ni^{2+}} + R_{NiOH^{+}} = 0 \tag{2-24}$$

Inclusion of Eq. (2-24) in the model ensures that there is instantaneous equilibrium between nickel and nickel hydroxide ions. Furthermore, the generation rate of nickel ions will balance hydrogen and hydroxyl ions. Therefore

$$R_{Ni^{2+}} + R_{H^{+}} - R_{OH^{-}} = 0 \tag{2-25}$$

Inclusion of Eq. (2-25) ensures that the hydrogen ions are in equilibrium with nickel and hydroxyl ions throughout the crevice region.

The divergence of flux of nickel and nickel hydroxide ions can be combined to yield

$$\nabla \cdot \left(N_{Ni^{2+}} + N_{NiOH^{+}}\right) = \frac{i_{Ni^{2+}}}{2F\mathrm{a}} \tag{2-26}$$

and the divergence of flux of nickel, hydrogen, and hydroxyl ions can be combined to yield

$$\nabla \cdot \left(N_{Ni^{2+}} + N_{H^{+}} - N_{OH^{-}}\right) = \frac{i_{Ni^{2+}}}{2Fa} \tag{2-27}$$

The concentration of nickel hydroxide in Eq. (2-24) is substituted with nickel and hydrogen ion concentration using Eq. (2-6). Similarly, the hydroxyl ion concentration in Eq. (2-25) is substituted with hydrogen ion concentration using Eq. (2-10).

The nonreacting species are chloride, nitrate, and sodium ions. The divergence of flux of chloride and nitrate ions are given by

$$\nabla \cdot N_{Cl^-} = 0 \tag{2-28}$$

and

$$\nabla \cdot N_{NO_3^-} = 0 \tag{2-29}$$

The concentration boundary conditions for these governing equations at the mouth of the crevice are given by Eq. (2-15). The electrolyte potential at the mouth of the crevice is assumed to be zero; that is

$$\Phi = 0 \tag{2-30}$$

At the end of the crevice, the electrolyte potential is represented by

$$\kappa \nabla \Phi + F \sum_{k=1}^{N} z_k D_k \nabla C_k = i_{Ni^{2+}} \tag{2-31}$$

Using Eq. (2-12), the boundary conditions for Eqs. (2-26) and (2-27) at the end of the crevice are

$$\left(N_{Ni^{2+}} + N_{NiOH^+} \right) \cdot \vec{n} = \frac{i_{Ni^{2+}}}{2F} \tag{2-32}$$

and

$$\left(N_{Ni^{2+}} + N_{H^+} - N_{OH^-} \right) \cdot \vec{n} = \frac{i_{Ni^{2+}}}{2F} \tag{2-33}$$

The flux boundary conditions at the end of the crevice for chloride and nitrate ions are

$$N_{Cl^-} \cdot \vec{n} = 0 \tag{2-34}$$

and

$$N_{NO_3^-} \cdot \vec{n} = 0 \tag{2-35}$$

An iterative procedure was used to solve Eqs. (2-23), (2-26), (2-27), (2-28), and (2-29), and the electroneutrality condition provided in Eq. (2-14), subjected to boundary conditions given by Eqs. (2-15) and (2-30)–(2-35). The governing equations are second-order ordinary differential equations with fixed boundary values at the mouth and at the end of the crevice. The equations were solved using the two-point boundary values solver function in MATLAB® (The MathWorks, Inc., 2008).

In the initial iteration, first, Eq. (2-23) is solved for potential distribution inside the crevice subjected to the boundary conditions given by Eqs. (2-30) and (2-31). The concentration distributions of various species inside the crevice is assumed to be equal to the bulk concentration. The solution of Eq. (2-23) provides the distributions of Φ, $\nabla\Phi$, and $\nabla^2\Phi$ inside the crevice. Second, the distributions of concentrations of chloride and nitrate ions are obtained by solving Eqs. (2-28) and (2-29) subjected to the boundary conditions given by Eqs. (2-15), (2-34), and (2-35). The solution of Eqs. (2-28) and (2-29) also provides the values of ∇C_{Cl^-}, $\nabla C_{NO_3^-}$, $\nabla^2 C_{Cl^-}$, and $\nabla^2 C_{NO_3^-}$ along the length of the crevice. Third, the distributions of nickel and hydrogen ion concentrations are obtained by solving Eqs. (2-26) and (2-27) subjected to the boundary conditions given by Eqs. (2-15), (2-32), and (2-33). The solution of Eqs. (2-26)

and (2-27) also provides the values of $\nabla C_{Ni^{2+}}$, ∇C_{H^+}, $\nabla^2 C_{Ni^{2+}}$, and $\nabla^2 C_{H^+}$ along the length of the crevice. Fourth, the distributions of concentrations of nickel hydroxide and hydroxyl ions and ∇C_{NiOH^+}, ∇C_{OH^-}, $\nabla^2 C_{NiOH^+}$, and $\nabla^2 C_{OH^-}$ are obtained using Eqs. (2-6) and (2-10). Fifth, the electroneutrality condition given by Eq. (2-14) is used to obtain the sodium ion concentration distribution, ∇C_{Na^+} and $\nabla^2 C_{Na^+}$ inside the crevice.

In the subsequent iterations, first, Eq. (2-23) is solved for potential distribution inside the crevice subjected to the boundary conditions given by Eqs. (2-30) and (2-31). The calculated values of concentration distribution from the previous iteration of various species are used to calculate κ in Eq. (2-23). Similarly, the calculated values of ∇C_k and $\nabla^2 C_k$ from the previous iteration are used to calculate $\nabla \kappa$ and $F\sum_{k=1}^{N} z_k \nabla \cdot (D_k \nabla C_k)$ which are part of Eq. (2-23). The second, third, fourth, and fifth steps in the initial iteration are repeated to obtain the concentration distributions, ∇C_k and $\nabla^2 C_k$ using the calculated values of Φ, $\nabla\Phi$, and $\nabla^2\Phi$ from the first step. The calculated values of the potential and concentration distributions are compared with the values from the previous iteration. If the absolute difference in potential and concentration distributions is less than a specified tolerance limit, the iterative procedure is terminated.

2.3 Model Parameters

The model is executed for the free corroding condition under which the metal potential, denoted by V, is equal to zero in Eq. (2-4). The value of the passive current density ($\bar{i}$), inverse of the Tafel slope (β) in Eq. (2-4), and equilibrium constants (K_{eq,N_i}, K_{H_2O}) in Eqs. (2-6) and (2-10) are provided in Table 2-2.

The value of the passive current density is obtained from experimental data collected for Alloy 22 in 1.0 M NaCl solution for this study. A cyclic polarization curve was obtained for the alloy in the solution according to ASTM G61 (ASTM International, 2003) at 95 °C [203 °F]. The polarization curve is presented in Figure 2-2. As seen in the figure, the measured current density is independent of potential in the forward scan; however, current density is a strong function of potential in the reverse scan. The data suggests that the metal surface was covered with a passive film while the alloy sample was anodically polarized in the forward scan. The current density is a strong function of potential in the reverse scan because original film was no longer in the passive state to protect the metal surface from corrosion. As seen in the figure, the passive current density is approximately equal to 2×10^{-6} A/cm^2 at an electrode potential equal to zero and the calculated value of the inverse of the Tafel slope (β) is 0.06 V^{-1}. The value of passive current density is the same as the one adopted by Watson and Postlethwaite, (1990). No assumption has been made regarding the presence or absence of passive film in the crevice region.

The values of equilibration constants for nickel ion hydrolysis reaction is adopted from Malki, et al. (2008), whereas, the dissociation constant for water is calculated using a thermodynamic calculator. These values are listed in Table 2-2. The values of diffusion coefficients of different species are calculated using the chemical thermodynamic simulator[13] (OLI Systems, Inc., 2010) and are provided in Table 2-3. The bulk concentrations of various chemical species also are provided in Table 2-3. The model is simulated for a 5-cm [1.97-in]-long and 0.5-mm [197-mils]-high crevice.

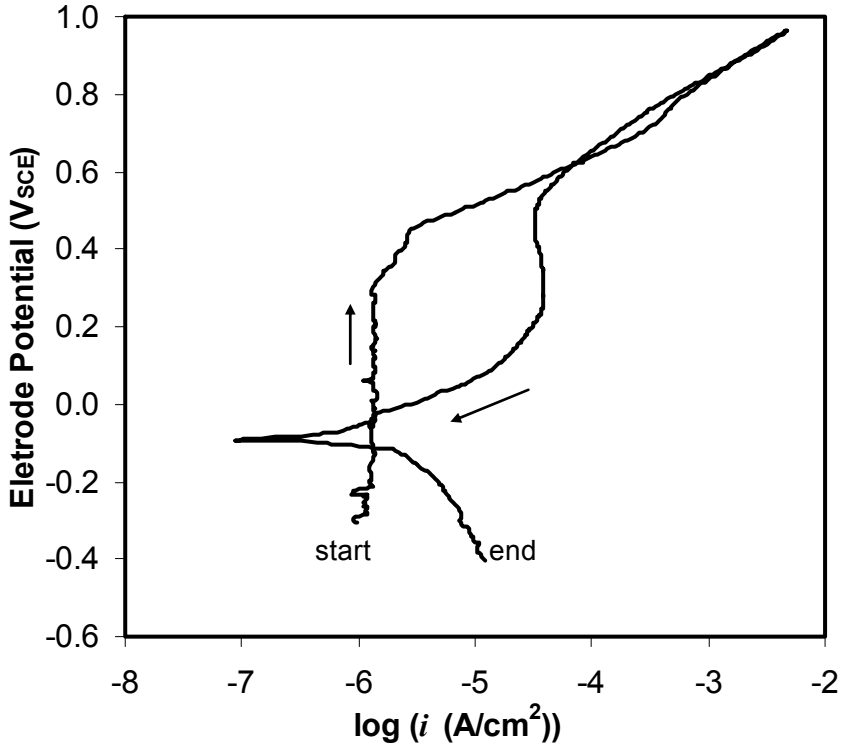

Figure 2-2. Potentiodynamic Polarization Curve for Alloy 22 in 1.0 M NaCl Solution at 95 °C [203 °F]

Table 2-2. Values of Parameters in Eqs. (2-4), (2-6), and (2-10)	
Parameter	**Values**
$\bar{i}$ (A/cm^2)	2×10^{-6}
β (V^{-1})	0.06
$K_{eq,Ni}$ (mol/cm^3)	1.38×10^{-13}
K_{H_2O} (mol^2/cm^6)	10^{-20}

Table 2-3. Diffusion Coefficients and Bulk Concentrations of Various Species in the Model		
Species	**Diffusion coefficient (cm^2/sec) at 95 °C**	**Concentration (mol/L)**
H^+	17.0×10^{-5}	10^{-8}
OH^+	11.9×10^{-5}	10^{-6}
Na^+	3.95×10^{-5}	Estimated using Eq. (2-14)
Cl^-	5.45×10^{-5}	0.5
NO_3^-	4.86×10^{-5}	0.1
Ni^{2+}	2.18×10^{-5}	10^{-6}
$NiOH^+$	2.15×10^{-5}	10^{-6}

2.4 Model Results

The calculated values of electrode potential ($V - \Phi$) are presented in Figure 2-3. As seen in the figure, the electrode potential becomes more cathodic with increasing distance. The electrode potential at the tip of the crevice is 9 mV more cathodic than at the mouth of the crevice. The calculated values of the nonreacting chemical species (chloride, nitrate, and sodium) are presented in Figure 2-4. As seen in the figure, the chloride, nitrate, and sodium ion concentrations increase with distance from the crevice mouth. Note that the ratio of nitrate to chloride ions remains constant throughout the crevice. This observation can be explained by analyzing the governing equations for the concentration distribution of chloride and nitrate inside the crevice. Because the divergence of flux of nitrate and chloride ions is zero throughout the crevice, the steady-state flux of nitrate and chloride ions is constant throughout the crevice, and

the transport properties, such as mobility and the diffusion coefficient of nitrate and chloride ions, have no impact on the steady-state concentration distribution inside the crevice. In fact, the concentration distribution of nitrate and chloride ions is only dependent on the gradient of potential distribution, $\nabla\Phi$, inside the crevice.

The concentration of nickel and nickel hydroxide ions as a function of distance is presented in Figure 2-5. As seen in the figure, the nickel ion concentration increases with distance from the crevice mouth, whereas the nickel hydroxide ion concentration first increases with distance up

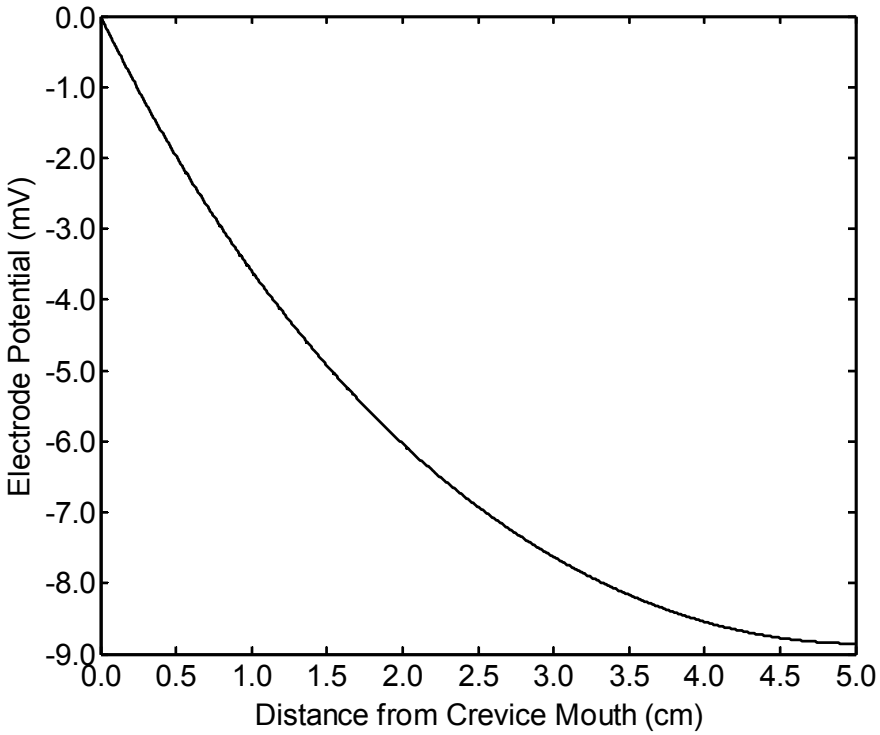

Figure 2-3. Electrode Potential ($V - \Phi$) as a Function of Distance From Crevice Mouth. The Potential Values Are With Respect to Standard Hydrogen Electrode.

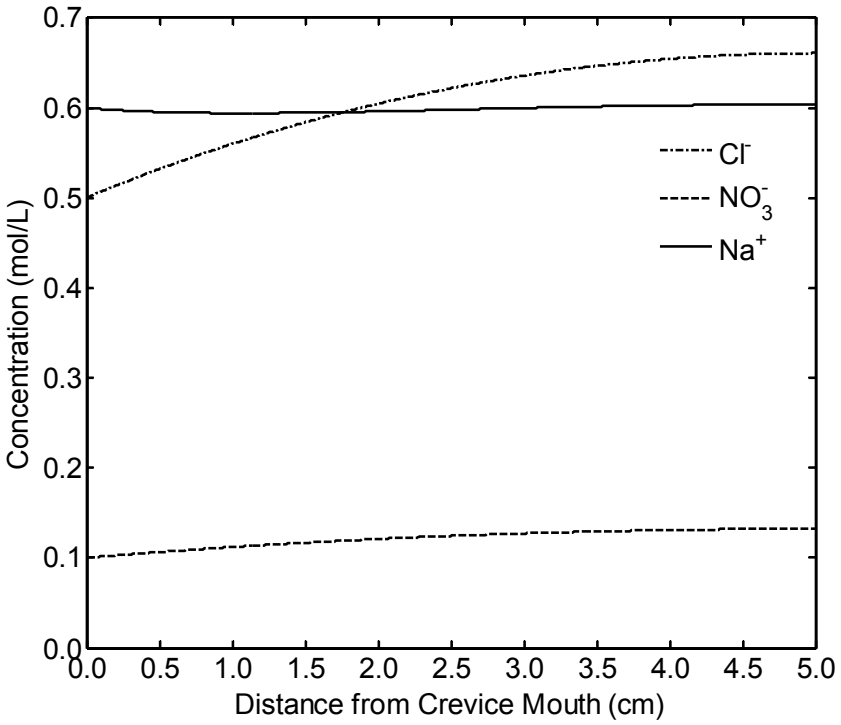

Figure 2-4. Concentration of Nonreacting Species (Chloride, Nitrate, and Sodium) as a Function of Distance From Crevice Mouth

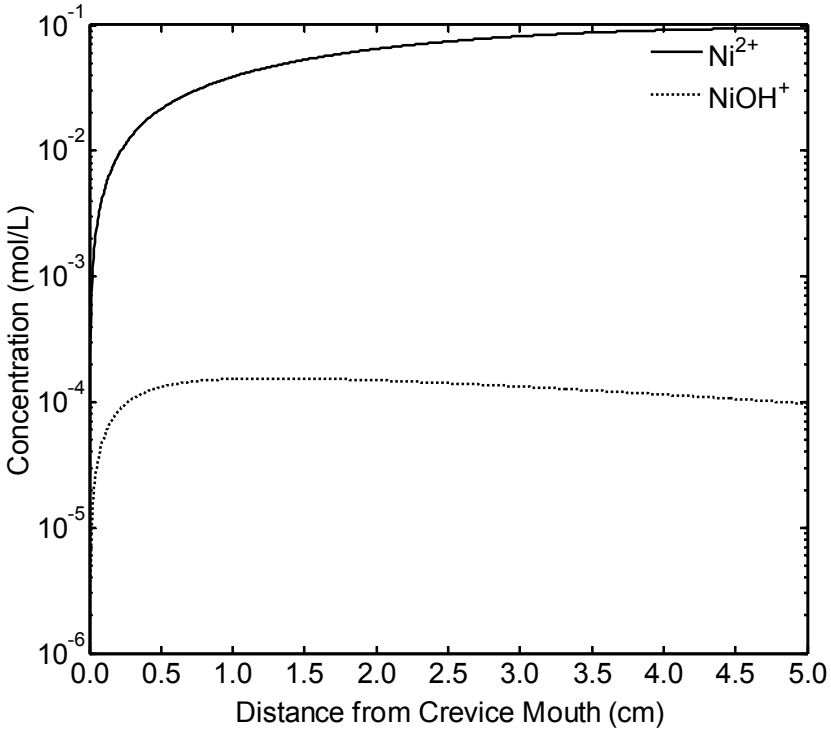

Figure 2-5. Concentration of Nickel and Nickel Hydroxide Ions as a Function of Distance From Crevice Mouth

to 1.0 cm [0.4 in] and then decreases with distance. The nickel ions are generated in the crevice as the potential becomes more cathodic. However, the nickel hydroxide ion concentration is determined by the equilibrium between the nickel, nickel hydroxide, and hydrogen ions.

The concentration of hydrogen and hydroxyl ions as a function of distance is presented in Figure 2-6. As seen in the figure, the hydrogen ion concentration increases with distance from the crevice mouth, whereas the hydroxyl ion concentration decreases with distance from the crevice mouth. The hydrogen ions are generated as nickel ions react with water to produce nickel hydroxide and hydrogen ions. An increased concentration of nickel ions corresponds to an increase in hydrogen ion concentration. Because the product of hydrogen and hydroxyl ion concentration is constant, the hydroxyl ion concentration decreases with distance from the crevice mouth. This result also indicates that the crevice solution is more acidic than the bulk solution due to generation of hydrogen ions.

The effect of different parameters' values on potential and concentration distributions was also studied. Two parameters, K_{eq,N_i} and $\bar{i}$, were independently varied. The value of K_{eq,N_i} was increased by three orders of magnitude and set to 1.38×10^{-10} mol/cm^3. The values of remaining parameters were the same as listed in Tables 2-2 and 2-3. It was observed that the electrode potential distribution was not affected by the change in K_{eq,N_i}. Similarly, the concentration distributions of nonreacting species (i.e., sodium, nitrate, and chloride ions) were also not affected by the change in K_{eq,N_i}. However, the concentration distributions of nickel and nickel hydroxide, hydrogen, and hydroxide ions are affected by the K_{eq,N_i} value. The concentration distributions of nickel and nickel hydroxide ions are presented in Figure 2-7(a),

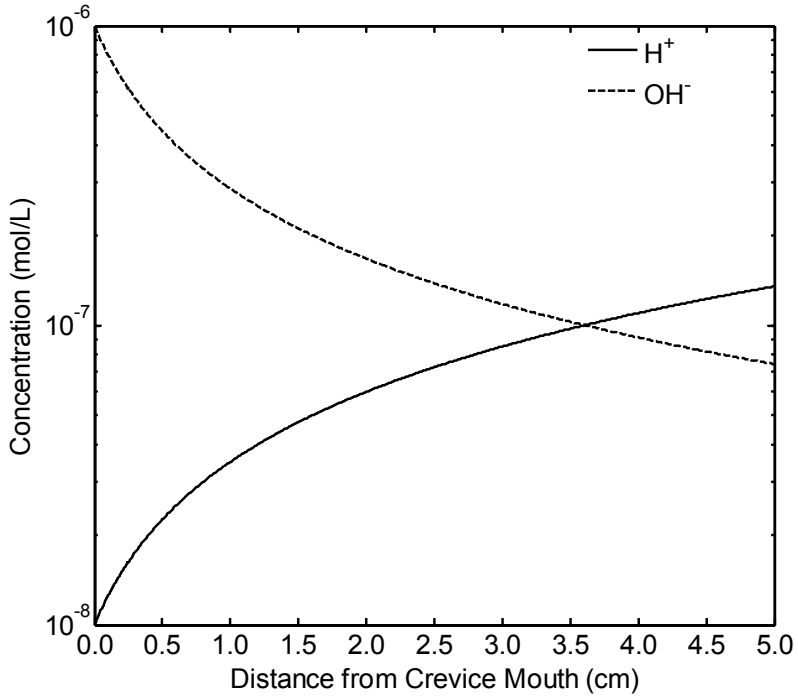

Figure 2-6. Concentration of Hydrogen and Hydroxyl Ions as a Function of Distance From Crevice Mouth

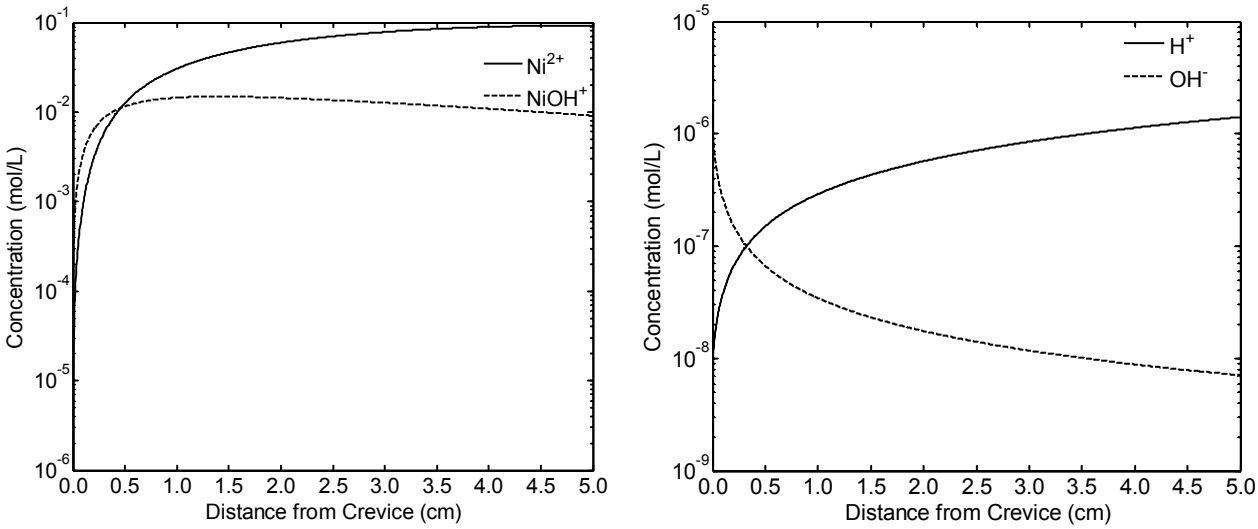

Figure 2-7. Concentration of (a) Nickel and Nickel Hydroxide Ions and (b) Hydrogen and Hydroxyl Ions as a Function of Distance From Crevice Mouth for K_{eq,N_i} Equal to 1.38×10^{-10} mol/cm^3. Remaining Parameters' Values Were the Same as Listed in Tables 2-2 and 2-3.

and of hydrogen and hydroxide ions are presented in Figure 2-7(b). Consistent with increased value of K_{eq,N_i}, the nickel hydroxide concentrations are higher along the crevice length compared to the K_{eq,N_i} value of 1.38×10^{-13} mol/cm^3. Similarly, the hydrogen ion concentrations are also higher for the increased value of K_{eq,N_i}. These simulation results also confirm that the model generates consistent results.

The model results for $\bar{i}$ equal to 10^{-4} A/cm^2 are presented in Figure 2-8. All other parameters' values are the same as listed in Tables 2-2 and 2-3. The selected value of $\bar{i}$ equal to 10^{-4} A/cm^2 is 50 times larger than $\bar{i}$ equal to 2×10^{-6} A/cm^2. As a result, the nickel dissolution rate is also higher. The model results reflect the higher dissolution rate of nickel. The electrode potential distribution is presented in Figure 2-8(a). As seen in the figure, the electrode potential varies between 0 to −90 mV with respect standard hydrogen electrode along the length of the crevice. The potential distribution in Figure 2-8(a) for $\bar{i}$ equal to 10^{-4} A/cm^2 is steeper than for $\bar{i}$ equal to 2×10^{-6} A/cm^2 (see Figure 2-3). The steeper potential distribution is also reflected in larger concentrations of nonreacting species (i.e., sodium ion, chloride, and nitrate), which are

presented in Figures 2-8(b), along the length of the crevice. Similarly, the higher value of $\bar{i}$ result in higher values of nickel and nickel hydroxide ions along the length of the crevice. The concentration distributions of nickel and nickel hydroxide ions are presented in Figure 2-8(c). The larger value of $\bar{i}$ results in higher dissolution rates of nickel, and thus, the higher concentration of nickel and nickel hydroxide ions along crevice length than for $\bar{i}$ equal to 2×10^{-6} A/cm^2 (see Figure 2-4). The higher concentrations of nickel hydroxide also results in higher values of hydrogen ion concentrations, which are presented in Figure 2-8(d), along the length of the crevice.

The following bullets provide a summary of the model results:

- The in-crevice solution is acidic compared to the bulk solution

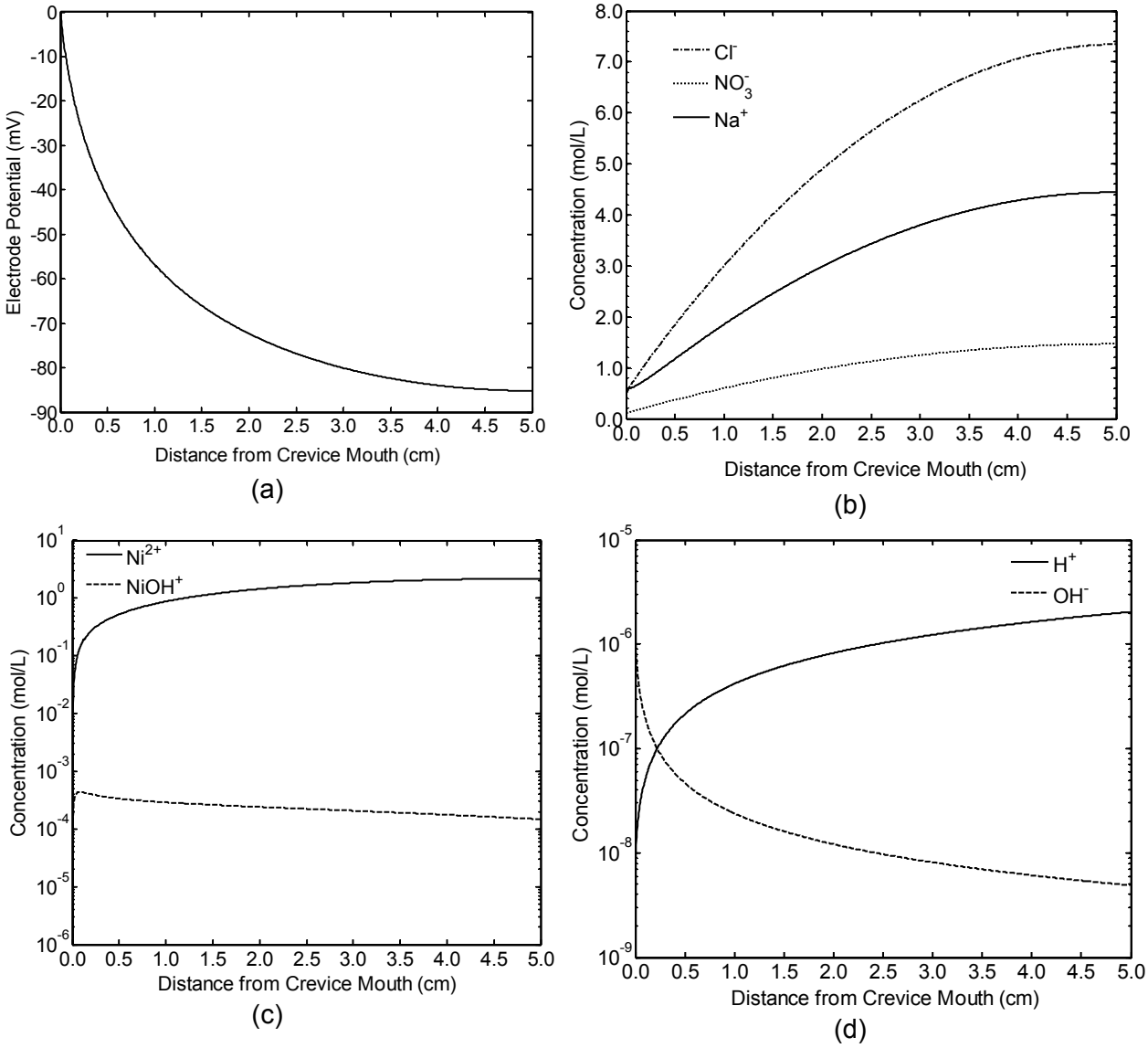

Figure 2-8. Distributions of (a) Electrode Potential with Respect to Standard Hydrogen Electrode; (b) Sodium, Chloride, and Nitrate Ions' Concentrations; (c) Nickel and Nickel Hydroxide Ions' Concentrations, and (d) Hydrogen and Hydroxyl Ions' Concentrations as a Function of Distance From Crevice Mouth for $\bar{i}$ Equal to 10^{-4} A/cm^2. Remaining Parameters' Values Are the Same as Listed in Tables 2-2 and 2-3.

- If nitrate and chloride are nonreacting, the ration of nitrate to chloride is the same as in the bulk

- An increase in $\bar{i}$ and K_{eq,N_i} results in an increase in pH of in-crevice solution

The model does not account for water reduction and hydrogen ion reduction reactions, which are expected to occur at cathodic potentials and in low pH solution. Similarly, the nitrate reduction reactions, which is expected to occur in low pH solutions, is not accounted for in the model. The model also does not account for complexation of chloride with nickel ions. Harb and

Alkarie (1991) considered complexation of nickel ions with chloride while simulating the in-crevice chemistry according to the following chemical reaction

$$Ni^{2+} + Cl^{-} \Leftrightarrow NiCl^{+} \qquad (2\text{-}35)$$

Harb and Alkarie, (1991) reported that the equilibrium constant for the reaction is approximately equal to 0.3 M^{-1}. This indicates that the reactant concentrations dominate at equilibrium. Therefore, most of the chlorides do not complexate with nickel ions. Moreover, the model predicted concentration of the nickel ions is an order of magnitude less than chloride concentration. For this reason, the complexation of nickel ions with chlorides is expected to be limited by the nickel ion concentration. Thus, the impact on chloride concentration due to the complexation reaction is not expected to exceed more than 30 percent. Thus, the model predicted chloride concentrations are expected to be approximately 30 percent more than expected chloride concentration if the complexation reaction was considered in the model.

Even though the model does not account for the nitrate reduction and nickel ion complexion reaction, the model predicted results are not far off from the expected values. Therefore, the ratio of nitrate to chloride is expected to be close to the bulk value. The model results are only indicative of evolution of in-crevice chemistry.

3 LITERATURE INFORMATION

As indicated by the model results, the in-crevice solution is expected to be more acidic that the bulk solution, and concentrations of nitrate and chloride is likely higher than the bulk. Moreover, the ratio of nitrate to chloride concentrations is not expected to be significantly different than the bulk. For this reason, literature information on corrosion of Alloy 22 in acidic chemical solutions containing chloride and nitrate was sought, and is provided next.

Llyod, et al. (2003) conducted polarization experiments on Alloy 22 in 1 M NaCl plus 0.1 M H_2SO_4 solution at various temperatures. The objective of the study Llyod, et al. (2003) conducted was to understand the effect of solution chemistry and temperature on stability of passive film of Alloy 22 in the solution. The calculated pH of the solution is 0.7. The test solutions were deaerated with ultrahigh purity argon for at least 20 minutes prior to starting the experiment, and this purge was continued throughout each experiment. Llyod, et al. (2003) conducted potentiostatic and potentiodynamic experiments at various temperatures. In the potentiostatic experiment, the Alloy 22 samples were polarized up to 700 mV with respect to Ag/AgCl reference electrode. The authors measured current density as a function of time in the potentiostatic experiments and measured current density as a function potential in the potentiodynamic experiments. Both experiments were conducted at various temperatures ranging from 25 to 85 °C [185 °F]. The authors reported that the Alloy 22 maintained low passive current density with a maximum of 2.0×10^{-6} A/cm^2 even at potential as high as 700 mV with respect to Ag/AgCl reference electrode at 85 °C [185 °F]. The authors concluded that even though the chemical composition of the passive film changed in the potentiostatic experiments at different temperatures, the film did not cease to exist at the metal surface.

Gray, et al. (2006a) tested the passivity of Alloy 22 over a broad range of pH and anion concentrations encompassing the aggressive solutions that may exist in these localized environments. The authors conducted experiments in 1 to 4 molal NaCl solution with varying amounts of acid. The authors used either HCl or H_2SO_4 or HNO_3 to adjust the pH of the NaCl solution. The amount of a selected acid was added such that the pH of the NaCl solution varied in the range of 2 to −1. The test solutions were purged with dissolved nitrogen to remove oxygen from the solution.

Gray, et al., (2006a) compared Alloy 22 corrosion rates as a function of pH for the different acids at 60 and 90 °C [140 and 184 °F] in a 1 molal NaCl , and 90 °C [184 °F] in a 4 molal NaCl solution. The authors defined passive film breakdown when corrosion rate equals or surpasses 100 µm/yr, and also critical pH when below which corrosion rate surpasses 100 µm/yr. The authors reported that the critical pH value changed with acid type and temperature. The authors' reported experimental results are summarized in Table 3-1.

Gray, et al. (2006a) reported that no critical pH was observed when acidity of the 1 and 4 molal NaCl solutions were adjusted using HNO_3. The authors conducted the measurements in the pH range of 2 to −0.7 for 1 molal NaCl solution at 60 and 90 °C [140 and 194 °F], and in the pH range of 3 to −0.4 for 4 molal NaCl solution at 90 °C [194 °F].

Gray, et al. (2006a) further reported that the breakdown of the passive film was evident in the corrosion potential of Alloy 22 samples in the test solutions. When pH of the 1 and 4 molal NaCl solutions were adjusted using HCl or H_2SO_4 , the corrosion potentials of the Alloy 22 samples remained virtually unchanged, whereas, the corrosion potential increased with decreasing pH when HNO_3 was used to the adjust pH of adjusted 1 and 4 molal NaCl solutions. Because the

Table 3-1. Critical pH in NaCl Solution for Alloy 22 Samples			
Acid Used to Adjust the pH	**Salt Concentration in Solution**	**Temperature (°C) [°F]**	**Critical pH***
HCl	1 molal NaCl	60 [140]	0.5
	1 molal NaCl	90 [194]	0.75
	4 molal NaCl	90 [194]	2.5
H_2SO_4	1 molal NaCl	60 [140]	0.5
	1 molal NaCl	90 [194]	0.6
	4 molal NaCl	90 [194]	2.5
*Critical pH, as defined by Gray, J.J., J.R. Hayes, G.E. Gdowski, B.E. Viani, and C.A. Orme. "Influence of Solution pH, Anion Concentration, and Temperature on the Corrosion Properties of Alloy 22." *Journal of the Electrochemical Society.* Vol. 153, No. 3. pp. B61–B67. 2006, below which the Alloy 22 corrosion rate surpasses 100 µm/yr.			

corrosion potentials of the Alloy 22 samples did not change with decreasing pH in HCl or H_2SO_4 adjust 1 and 4 molal NaCl, the rate of hydrogen ion reduction reaction increased with decreasing pH. As a result, the oxidation rates of metal species present in Alloy 22 also increased with decreasing pH. Thus, the overall corrosion rate increased with pH decrease.

Gray, et al. (2006b) conducted additional studies to understand the effect of nitrate and chloride concentrations and nitrate to chloride ratio in low pH solution on Alloy 22 corrosion rates. The authors conducted experiments with Alloy 22 samples immersed in solution containing NaCl and KNO_3 salts. The NaCl concentration in the solutions was either 1 or 4 molal. Appropriate amounts of KNO_3 was added to achieve desired values of $[NO_3^-]/[Cl^-]$. Acidity of a test solution was varied by adding an HCl-HNO_3 acid solution. The acid solution had the same $[NO_3^-]/[Cl^-]$ as the test solution whose acidity was varied by adding the acid solution. The corrosion rate of Alloy 22 samples were measured as a function of test solutions' pH. The corrosion potentials of the Alloy 22 samples were also recorded. The corrosion experiments were conducted at 60 and 90 °C [140 to 194 °F] The test solutions were continuously purged with nitrogen to remove dissolved oxygen.

Gray, et al. (2006b) first conducted a control experiment in HCl solution with varying pH at 90 °C [194 °F]. The Alloy 22 corrosion rates remained below 20 µm/yr until the HCl solution pH was greater than 1. The alloy corrosion rates suddenly increased when pH approximately was equal to 1. The measured corrosion potentials of the alloy remained between 0 and −0.2 V versus Ag/AgCl in the entire solution pH ranges. The authors concluded that the critical pH in the HCl solution was approximately equal to 1. Gray, et al. (2006b) conducted a series of Alloy 22 corrosion rate measurements in 1 and 4 molal NaCl solutions. Potassium nitrate was added in the NaCl solutions to obtain a desired value of $[NO_3^-]/[Cl^-]$. The acidity, and thus pH, of the solutions was varied by adding the acid solutions. The authors reported that in 1 molal NaCl plus 0.05 molal KNO_3 solution with $[NO_3^-]/[Cl^-]$ equal to 0.05, corrosion rate first increased and then decreased with the solution pH in the range of 0.5 to −0.2. The peak corrosion rate of Alloy 22 in the 1 molal NaCl plus 0.05 molal KNO_3 solution is between 20 to 40 µm/yr at pH approximately equal to 0. The authors concluded that small concentrations of nitrate control the runaway corrosion rate, which was observed with the HCl solution, of Alloy 22. Gray, et al. (2006b) conducted additional tests in 1 molal NaCl plus 0.2 molal KNO_3 and 1 molal NaCl plus 0.5 molal KNO_3 solutions. The author reported that the transpassive dissolution of the alloy took place in both the solutions below pH equal to 1.0. Though, the rate of dissolution, and thus

the corrosion rate, was lower in 1 molal NaCl plus 0.5 molal KNO_3 solution compared to 1 molal NaCl plus 0.2 molal KNO_3 solution. The corrosion rate data reported by Gray, et al. (2006b) is summarized in Table 3-2.

Gray, et al. (2006b) also conducted corrosion rate measurements of Alloy 22 in 4 molal NaCl solution with varying amount of KNO_3. These experiments enabled the authors to evaluate the effect of chloride concentration on corrosion rate of Alloy 22 in low pH solutions. The corrosion rates of Alloy 22 in 4 molal NaCl plus 0.2 molal KNO_3 solution with $[NO_3^-]/[Cl^-]$ equal to 0.05 first increased and then decreased in the pH range of 1.5 to 0.5. The peak corrosion rate was approximately equal to 20 µm/yr at about pH of 1. The corrosion rate of the alloy exponentially increased when pH was less than 0.5. The authors concluded that, similar to 1 molal NaCl plus 0.05 molal KNO_3 solution, small additions of nitrate ions control the runaway corrosion of Alloy 22 observed in the HCl solution. The authors further concluded that transpassive dissolution of the alloy took place in the solution below pH equal to less than 0.5. When compared with 1 molal NaCl plus 0.05 molal KNO_3, the critical pH for transpassive dissolution increased from 0 to 0.5 in the 4 molal NaCl plus 0.2 molal KNO_3 solution. Similarly, the critical pHs for transpassive dissolution were approximately equal to 1 in 4 molal NaCl plus 0.8 molal KNO_3 and 4 molal NaCl plus 2.0 molal KNO_3 solutions, whereas critical pHs were −0.15 and −0.25 in 1 molal NaCl plus 0.2 molal KNO_3 and 1 molal NaCl plus 0.5 molal KNO_3 solutions, respectively. These experiments further affirmed the conclusion that increase in chloride concentration results in increase of critical pH for transpassive dissolution. Furthermore, presence of nitrate only decreases the critical pH below which transpassive dissolution takes place. Thus, in presence of nitrate ions, a more acidic environment is needed to initiate transpassive dissolution of the alloy in a solution containing nitrate compared to a solution without nitrate.

The presence of other localized corrosion inhibiting anions, such as sulfate, may also further decrease critical pH below which transpassive dissolution takes place. Ilevbare, et al. (2005) reported that nitrate is the most effective anion that affects the localized corrosion repassivation potential. Brossia and Kelly (1998) reported that nitrate is 65 times more effective than sulphate in the inhibition of crevice corrosion on SS 304. Thus, the presence of other localized-corrosion-inhibiting anions is not expected to significantly change the critical pH.

Table 3-2. Gray, et al.* Reported Corrosion Rate and Corrosion Potential Data for Alloy 22 in Different Solutions

Solution	pH Range	Corrosion Rate Data	Corrosion Potential Data	Summary
HCl solution	2 to 1	Below 20 µm/yr until pH >1, corrosion rate suddenly increased when pH ≤1	Corrosion potential remained between 0 and −0.2 V vs. Ag/AgCl	Critical pH was approximately equal to 1.
1 molal NaCl plus 005 molal KNO_3.solution with $[NO_3^-]/[Cl^-]$ equal to 0.05. pH was adjusted by adding HCl–HNO_3 mixture	2 to −0.25	Corrosion rate first increase and then decreases with pH in the range of 0.5 to −0.2. The peak corrosion rate is between 20 to 40 µm/yr at about pH equal to 0.	Corrosion potential increases with decreasing pH.	Small concentrations of nitrate ions control the runaway corrosion rate, which was observed with HCl solution, of Alloy 22.

Table 3-2. Gray, et al.* Reported Corrosion Rate and Corrosion Potential Data for Alloy 22 in Different Solutions (continued)				
Solution	**pH Range**	**Corrosion Rate Data**	**Corrosion Potential Data**	**Summary**
1 molal NaCl plus 0.2 molar KNO_3 solution with $[NO_3^-]/[Cl^-]$ equal to 0.2. pH was adjusted by adding $HCl–HNO_3$ mixture	2 to −0.4	Corrosion rate remains constant till pH is lowered to approximately −0.15. Corrosion rate then increases exponentially with decreasing pH.	Corrosion potential increases linearly with decreasing pH. The rate of increase is higher when pH is below 0.5.	Alloy 22 sample remains passive in the solution till the pH is lowered to −0.15.
1 molal NaCl plus 0.5 molal KNO_3 solution with $[NO_3^-]/[Cl^-]$ equal to 0.5. pH was adjusted by adding $HCl–HNO_3$ mixture	2 to −0.4	Corrosion rate remains constant till pH is lowered to approximately equal to −0.25. Corrosion rate then increases rapidly, but not exponentially, with decreasing pH.	Corrosion potential increases linearly with decreasing pH. The rate of increase is higher when pH is below 1.0.	Alloy 22 sample remains passive in the solution till the pH is lowered to −0.25. The rate of increase is not as high as one observed for $[NO_3^-]/[Cl^-]$ equal to 0.2.
4 molal NaCl plus 0.2 molal KNO_3.solution with $[NO_3^-]/[Cl^-]$ equal to 0.05. pH was adjusted by adding $HCl–HNO_3$ mixture	3 to −0.25	Corrosion rate first increase and then decreases with pH in the range of 1.5 to 0.5. The peak corrosion rate is approximately 20 µm/yr at about pH of 1.0. Corrosion rate exponentially increases when pH <0.5.	Corrosion potential increases linearly with decreasing pH. The rate of increase is higher when pH is below 1.0.	Similar to 1 molal NaCl plus 0.05 molal KNO_3 solution, small additional of nitrate ions control the runaway corrosion rate, which was observed with HCl solution, of Alloy 22.
4 molal NaCl plus 0.8 molar KNO_3 solution with $[NO_3^-]/[Cl^-]$ equal to 0.2. pH was adjusted by adding $HCl–HNO_3$ mixture	3 to −0.25	Corrosion rate remains constant till pH is lowered to 1.0. Corrosion rate then increases exponentially with decreasing pH.	Corrosion potential increases linearly with decreasing pH. The rate of increase is higher when pH is below 0.5.	Alloy 22 sample remains passive in the solution till the pH is above 1.0. Transpassive dissolution takes place below pH 1.0.
4 molal NaCl plus 2.0 molal KNO_3 solution with $[NO_3^-]/[Cl^-]$ equal to 0.5. pH was adjusted by adding $HCl–HNO_3$ mixture	2 to −0.4	Corrosion rate remains constant till pH is lowered to 1.0. Corrosion rate then increases exponentially with decreasing pH.	Corrosion potential increases almost linearly with decreasing pH. The rate of increase is higher when pH is below 0.5.	Alloy 22 sample remains passive in the solution till pH is above 1.0. Transpassive dissolution takes place below pH 1.0. The corrosion rate is similar to one observed for 4 molal NaCl plus 0.8 molar KNO_3 solution with $[NO_3^-]/[Cl^-]$ equal to 0.2.

*Gray, J. J., J. R. Hayes, G. E. Gdowski, B. E. Viani, and C. A. Orme. "Inhibiting Effects of Nitrates on the Passive Film Breakdown of Alloy 22 in Chloride Environments." *Journal of The Electrochemical Society.* Vol. 153, No. 5. pp. B156–-B161. 2006.

4 SUMMARY AND CONCLUSIONS

A physico-chemical process model for a steady-state chemical environment inside a crevice for nickel-based alloys is presented. The model accounts for one heterogeneous and two homogeneous chemical reactions. The heterogeneous chemical reaction is the dissolution of nickel metal, and two homogeneous chemical reactions are the hydrolysis of nickel ions, resulting in formation of nickel hydroxide and hydrogen ions and, the dissociation of water. The concentration and potential variations along the crevice width are assumed to be negligible compared to the crevice length. The governing steady-state equations for the potential and concentration distributions of various species are algebraically simplified and then solved using an iterative procedure.

The model is simulated for parameter values provided in Section 2.3. The calculated results are presented in the form of potential and concentration distributions of various species as a function of distance from the crevice mouth. The model results indicate that electrode potential becomes more cathodic along the crevice length measured from the crevice mouth. The calculated potential distribution inside the crevice is consistent with the results presented by Song and Sridhar (2008) and Allahar (2003) that showed that the potential becomes more cathodic inside a crevice.

The calculated results also show that the concentrations of nonreacting anionic species (chloride and nitrate) increase with distance from the crevice mouth. Note that the ratio of concentration of nitrate to chloride ions remains constant throughout the crevice length. This result is consistent with the fact that the concentration distributions of nitrate and chloride ions are solely dependent upon the gradient of potential inside the crevice and are independent of the diffusion coefficient and mobility of the ions.

The concentrations of nickel and hydrogen ions increase with distance from the crevice mouth. The nickel hydroxide ion concentration increases with distance from the crevice mouth up to 1.0 cm [0.4 in] and then decreases thereafter. The hydroxyl ion concentration decreases with distance from the crevice mouth. The concentration profile of nickel ion is consistent with the fact that nickel ions are generated by the dissolution of metal throughout the crevice, and nickel ions are transported along the crevice depth to balance the ionic charge accumulated because of increased concentration of chloride and nitrate ions. The increase of hydrogen ion concentration is consistent with the fact that the nickel ions react with water molecules to produce hydrogen ions. Therefore, a high concentration of nickel ions corresponds to a high concentration of hydrogen ions. The concentration of nickel hydroxide ions is determined by the interplay between the equilibrium constants denoted by K_{eq,N_i} and K_{H_2O} in Eqs. (2-6) and (2-10), respectively. The concentration of hydroxyl ions decrease throughout the crevice because the K_{H_2O} for the water dissociation reaction is constant throughout the crevice and the hydrogen ion concentration increases with distance from the crevice mouth.

The physico-chemical process model does not account for several heterogeneous reactions, such as nitrate and water reduction reactions, and dissolution of other chemical species, such as chromium and iron, present in Alloy 22. Moreover, the model also does not account for complexation of chloride with nickel ions reaction that Harb and Alkarie (1991) considered. Additional analyses using literature information indicated that the exclusion of nitrate reduction and the complexation reactions in the model is not expected to significantly alter nitrate to chloride ratio compared to the bulk value.

The literature information indicated that the transpassive dissolution of Alloy 22 at corrosion potential could take place as long as solution surrounding the alloy is acidic enough (i.e., the solution pH is below a critical value). Moreover, the presence of nitrate and other localized corrosion inhibiting anions is only expected to decrease critical pH below which transpassive dissolution takes place. The physico-chemical model results indicate that the in-crevice solution is expected to be more acidic than the bulk solution. The actual acidity of the solution will depend upon rate of nickel dissolution and nickel ion hydrolysis reactions. The model results also indicate that in-crevice solution pH decreases with distance from crevice mouth. This suggests that the lowest pH in-crevice solution is expected to reside farthest from the crevice mouth. An analysis of model results in view of literature information indicates that more acidic chemical environment could evolve inside a crevice than predicted by the model. The model is simulated for a fixed value of equilibrium current density ($\bar{i}$ in Eq. 2-4) associated with dissolution of the nickel. The literature information indicates that the corrosion rate of the alloy increases with decreasing pH. Therefore, it is most likely that equilibrium current density will increase along the crevice from the crevice mouth. This could result in evolution of in-crevice solutions with pHs below the threshold pH for transpassive dissolution of the alloy. The combined analysis of the model results and literature information suggests that the stifling of crevice corrosion solely based upon in-crevice chemistry is not credible.

5 REFERENCES

Alkire, R. and D. Siitari. "The Location of Cathodic Reaction During Localized Corrosion." *Journal of the Electrochemical Society*. Vol. 126, No. 1. pp. 15–22. 1979.

Allahar, K. "Mathematical Modeling of Disbonded Coating and Cathodic Delamination Systems." Ph.D. dissertation. University of Florida. Florida, Gainesville. 2003.

ASTM International. "Standard Test Method for Conducting Cyclic Potentiodynamic Polarization Measurements for Localized Corrosion Susceptibility of Iron-, Nickel-, or Cobalt-Based Alloys." ASTM G61-86. West Conshohocken, Pennsylvania: ASTM International. 2003.

Baes, J. and W. Mesmer. *The Hydrolysis of Cations*. New York City, New York: John Wiley & Sons. 1979.

Brossia, C.S. and R.G. Kelly. "Influence of Alloy Sulfur Content and Bulk Electrolyte Composition on Crevice Corrosion Initiation of Austenitic Stainless Steel." *Corrosion*. Vol. 54. p. 145. 1998.

Chiang, K.T., D.S. Dunn, Y.-M. Pan, O. Pensado, and P. Shukla. "Stress Corrosion Cracking of Waste Package Material Modeling and Experiments." CNWRA 2007-01. San Antonio, Texas: CNWRA. 2007.

DOE. DOE/RW–0573, "Yucca Mountain Repository License Application." Rev. 0. ML081560400. Las Vegas, Nevada: DOE, Office of Civilian Radioactive Waste Management. 2008.

——— DOE/RW–0539–1, "Yucca Mountain Science and Engineering Report: Technical Information Supporting Site Recommendation Consideration." Rev. 1. Las Vegas, Nevada: DOE, Office of Civilian Radioactive Waste Management. 2002.

Dunn, D.S., O. Pensado, Y.-M. Pan, R.T. Pabalan, L. Yang, X. He, and K.T. Chiang. "Passive and Localized Corrosion of Alloy 22–Modeling and Experiments." CNWRA 2005-02. Rev. 1. San Antonio, Texas: Center for Nuclear Waste Regulatory Analyses. 2005.

Evitts, R.W., M.M.A. Gad, M.K. Watson, and J. Postlethwaite. "Crevice Corrosion of Nickel Alloys at Elevated Temperatures: Experimental and Modeling Studies." CORROSION/93 Paper No. 601. Houston, Texas: NACE. pp. 601:1–601:10. 1993.

Gordon,G.M. "Corrosion Considerations Related to Permanent Disposal of High-Level Radioactive Waste." *Corrosion*. Vol. 58. pp. 811–825. 2002.

Gray, J.J., J.R. Hayes, G.E. Gdowski, B.E. Viani, and C.A. Orme. "Influence of Solution pH, Anion Concentration, and Temperature on the Corrosion Properties of Alloy 22." *Journal of the Electrochemical Society.* Vol. 153, No. 3. pp. B61–B67. 2006a.

———. "Inhibiting Effects of Nitrates on the Passive Film Breakdown of Alloy 22 in Chloride Environments." *Journal of the Electrochemical Society.* Vol. 153, No. 5. pp. B156–B161. 2006b.

Harb, J.N. and R.C. Alkire. "Transport and Reaction During Pitting Corrosion of Ni in 0.5M NaCl. Stagnant Fluid." *Journal of the Electrochemical Society*. Vol. 138. pp. 2,594–2,600. 1991.

He, X. and D.S. Dunn. "Crevice Corrosion Penetration Rates of Alloy 22 in Chloride-Containing Waters." *Corrosion*. Vol. 63. pp. 145–158. 2007.

He, X., D.S. Dunn, and C.S. Csontos. "Corrosion of Similar and Dissimilar Metal Crevices in the Engineered Barrier System of a Potential Nuclear Waste Repository." *Electrochimica Acta*. Vol. 52. pp. 7,556–7,569. 2007.

Hoffmeister, H. "Modeling Crevice Corrosion of Pure Nickel by Coupling of Phase and Polarization Behavior at Various pH, Chloride, and Oxygen Levels." CORROSION/2004 Paper No. 04289. Houston, Texas: NACE. 2004.

Hua, F. and G. Gordon. "Corrosion Behavior of Alloy 22 and Ti Grade 7 in a Nuclear Waste Repository Environment." *Corrosion*. Vol. 60. pp. 764–777. 2004.

Ilevbare, G.O., K.J. King, S.R. Gordon, H.A. Elayat, G.E. Gdowski, and T.S.E. Gdowski. "Effect of Nitrate on the Repassivation Potential of Alloy 22 in Chloride-Containing Environments." *Journal of the Electrochemical Society*. Vol. 152, No. 12. pp. B547–B554. 2005.

Kirk, R. E. and D.F. Othmer. "Encyclopedia of Chemical Technology." Vol. 17. 4th Edition. New York City, New York: Wiley International. 1997.

Lloyd, C., D.W. Shoesmith, N.S. McIntyre, and J.J. Noel. "Effects of Temperature and Potential on the Passive Corrosion Properties of Alloys C22 and C276." *Journal of the Electrochemical Society*. Vol. 150. pp. B120–B130. 2003.

Malki, B., T. Souier, and B. Baroux. "Influence of the Alloying Elements on Pitting Corrosion of Stainless Steels: A Modeling Approach." *Journal of the Electrochemical Society*. Vol. 155, No. 12. pp. C583–C587. 2008.

OLI Systems, Inc. "A Guide to Using the OLI Software for Version 3.1 of the Analyzers." Morris Plains, New Jersey: OLI Systems, Inc. 2010.

Priyantha, N., P. Jayaweera, G.R. Englehardt, A. Davydov, and D.D. Macdonald. "Localized Corrosion of Alloy 22 in Sodium Chloride Solutions at Elevated Temperature." *Corrosion*. Vol. 61. pp. 857–871. 2005.

Song, F.M. and N.Sridhar. "Modeling Pipeline Crevice Corrosion Under a Disbonded Coating With or Without Cathodic Protection Under Transient and Steady State Conditions." *Corrosion Science*. Vol. 50. pp. 70–83. 2008.

The MathWorks, Inc. "MATLAB Version 7.7.0.471 (R20008b)." Natick, Massachusetts: The MathWorks, Inc. 2008.

Watson, M. and J. Postlethwaite. "Numerical Simulation of Crevice Corrosion of Stainless Steels and Nickel Alloys in Chloride Solutions." *Corrosion*. Vol. 46. pp. 522–530. 1990.